Case Studies in Construction Materials 18 (2023) e01844

Contents lists available at ScienceDirect

Case Studies in Construction Materials

journal homepage: www.elsevier.com/locate/cscm

Microcracking monitoring and damage detection of graphene nanoplatelets-cement composites based on acoustic emission technology

Shahzad Ashraf [a,*], Suliman Khan [b], Vipin Kumar Oad [c]

[a] Department of Mechanics of Materials and Structures, Faculty of Civil and Environmental Engineering, Gdańsk University of Technology, Narutowicza 11/12, 80–233 Gdańsk, Poland
[b] Department of Civil Engineering, NFC, IEFR, Faisalabad, Pakistan
[c] Gdańsk University of Technology, Faculty of Civil and Environmental Engineering, Gdańsk, Poland

ARTICLE INFO

Keywords:
Graphene nanoplatelets
Cement composites
Microcracking monitoring
Mechanical degradation
Acoustic emission analysis

ABSTRACT

This study aims to identify the micro-cracking pattern and structural applications of cement composites replaced with 0 wt%, 0.04 wt%, and 0.08 wt% contents of graphene nanoplatelets (GNPs) over cement weight through acoustic emission (AE) monitoring under mechanical degradation. The ultraviolet-visible spectroscopy (UV–vis) results showed that at 60 min sonication period, GNP-4 showed maximum absorbance rate of 16.15% compared to the GNP-8. The microstructural characteristics revealed that during hydration of cement there was no apparent cracks appeared in GNPs-cement composites compared to the reference specimen (GNP-0) which was 1.44 mm. The cracking mode and damaged detection of the tested specimens resulted in three distinct stages i.e., (I) pre-peak, (II) peak, and (III) post-peak under mechanical degradation. GNP-4 achieved 780 N flexural capacity which was increased by 30% and 21.87% compared to the GNP-0 and GNP-8. Similarly, a compressive strength of 63.12 MPa, 57.5 MPa, and 56 MPa at 28 days was obtained by GNP-4, GNP-8, and GNP-0, respectively. Based on AE hits and amplitude analysis, the resistance to fracture, damping capacity, and ductility of GNP-4 was improved by 25.30%, 25.1%, and 22.47% respectively, to that of GNP-0. Shear failure (>35 kHz) was observed in GNP-0, while GNPs cement composites recorded tensile failure (<35 kHz) through RA-AF parameters. The cracking pattern through Ib value with a warning sign of 1.5 between micro and macro-cracks and severity of damages through historical index (HI) and severity index (Sr) of GNPs cement composites was determined. Lastly, it was concluded that GNPs contents can significantly improve bending strength and delay the cracks initiation in cement composites.

1. Introduction

Cement composites are one of the most common materials used in civil engineering construction; however, as the modern construction industry has grown, and rely on advanced cement composites which provides excellent mechanical properties, resistance, and durability against the applied loading [1]. Several inadequacies such as mechanical performance and environmental impacts with cement prevent it from being used proficiently as a construction material. The primary weakness is its inherent brittleness and poor

* Corresponding author.
E-mail address: shahzad.ashraf@pg.edu.pl (S. Ashraf).

https://doi.org/10.1016/j.cscm.2023.e01844
Received 19 September 2022; Received in revised form 27 December 2022; Accepted 6 January 2023
Available online 9 January 2023

tensile strength of the material, both caused by flaws and microcracks. Such microcracks and apparent damages in concrete structures are caused by excessive water, plastic settlement, bleeding, and shrinkage [2,3]. These premature defects propagate and coagulate under applied loads, resulting in microcracks that cause mechanical destabilization and eventually lead to catastrophic failure of concrete structures. With the advancement in nanotechnology, the cited drawbacks can be overcome by incorporating several types of reinforcing materials in cement composites, including steel fibre [4], carbon nanofibers (CNFs) [5], carbon nanotubes (CNTs) [6], graphene [7], nano silica [8], nano clay [9], and nanosized titanium dioxide (TiO_2) [10]. These nanomaterials have contributed to increase the cement composites tensile strength, fracture resistance, and toughness at the nanoscale level. Graphene, a single sheet of graphite, has recently become a significant research priority due to its potential use as a nanomaterial reinforced in cement composites. Graphene is a useful nano-structural material with high fracture strength (130 GPa), Young's modulus (~1 TPA), intrinsic mobility ($200{,}000 cm^2v^{-1}s^{-1}$), lightweight(1 g/cm^3), a large theoretical specific surface area (2630 m^2/g), its optical transmittance (~97.7%), and its capacity to absorb 10% more energy than steel before the actual failure. These unique characteristics have made graphene more popular for research and development than other reinforcing materials[11]. The two-dimensional carbon structures known as graphene nanoplatelets (GNPs) have single or multiple layers of graphite planes. GNPs are not affected by agglomerations, in contrast to one-dimensional carbon nanotubes, which are vulnerable to agglomerations [12,13]. GNPs facilitate higher interaction with the surrounding hydration products because of the larger surface area and excellent surface structure. Due to its two-dimensional plate-like structure, it deviates the fracture path, prevents crack initiation and delays crack propagation [14]. Numerous research has been carried out where finely grained nanoparticles GNPs have been employed in cement/mortar composites to enhance the mechanical characteristics and sensing the ability of cementitious composites and the ductility of concrete [15–17]. Qiong Liu et al. [14] reported that the incorporation of GNPs in cement mortar led to a 36% increase in the compressive strength of nano reinforced cement-mortar. Chen et al.[18] investigated the addition of GNPs in concrete mix at a proportion of 0.05 wt% enhanced compressive strength by 22%, while a considerable decline in compressive strength has been observed on the further addition of GNPs. Wang et al. [19] and Alkhateb et al.[20] concluded that the introduction of the GNPs in cement composites speeds up the heat of the hydration process resulting in a higher density (C-S-H gel), and ultimately improves the mechanical performance. Furthermore, Zheng et al. [21] and Jaitanong et al. [22] investigated in their research that incorporating graphene-based materials in cement composites minimizes the possibility of cracking at the early stage of construction.

The existence of cracks in concrete structures has a substantial influence on the structural safety and long-term durability of the structures. To support sustainability, quality-of-life standards, and economic prospects, the non-destructive evaluation (NDE) method is used for smart health monitoring of numerous structures and infrastructural systems [23]. Acoustic emission (AE), defined as the emission of strain energy in the form of transient elastic waves, is a well-known NDE tool used to analyse the damage detection and assessment of different types structures [24,25]. To measure the damage in concrete structures, numerous researchers have categorised several AE parameters in their research. Many researchers have focused on analyzing the basic characteristics of AE signals, such as their counts, rise time, hits, amplitude, energy, signal intensity, and frequency [23]. E. Proverbio et al. [25] introduced a wide range of AE parameter techniques in their research to investigate the deterioration of reinforced concrete structures. Elfergani et al. [26] investigated the identification and evaluation of damage in a prestressed concrete structure through AE technology.

Several analytical methods based on AE signals were used to analyze the damage processes and failure modes of concrete structures, including the b-value method, average frequency (AF) vs. RA value, and AE signal intensity analysis. In compression and shear failures, which primarily result in shear cracks, most AE signals have a low average frequency (AF) and a high value of (RA). In contrast, bending and tensile failures primarily result in a tensile crack and have a maximum average frequency (AF) and a low range of (RA) [27]. To carry out AE signal analysis, few scholars used the b-value analysis approach [28,29]. Shiotani et al. [30] introduced the Ib-value method to better understand fatigue crack nucleation following the propagation of tensile cracks. Sagar et al. [31] examined the propagation of different fatigue crack phases in concrete by using the b-value method. Numerous studies concluded that the b-value analysis would be useful in understanding the inherent microscopic processes of fracture mechanics [32,33]. AE technology is now being utilized in fracture identification of concrete columns [34], concrete beams [35] and composite materials[36]. Also, the AE signal intensity analysis (IA) can be used to characterize the level of damage incurred by a concrete structure [23]. Nair et al. [37] utilized the AE intensity analysis approach while researching reinforced concrete (RC) members. The IA plot of a historical index (HI) vs. severity (Sr) correlates well with specimen damage and shows a promising correlation. In the assessment of concrete structures, the crack intensity parameters HI and Sr have been utilized by a large number of researchers [38,39].

Although, few studies have been conducted on the mechanical performance and micro-cracking monitoring of GNPs-cement composites under AE technology. However, no significant investigation has been carried out on the structural applications of GNPs in different kinds of concrete structures which are under extreme loading. Because of the strong interlocking bond as revealed by FESEM study, the GNPs cement composites can be a good alternative of Ordinary Portland cement mortar in hot regions where control of dry shrinkage and delay in cracks initiations are required. Therefore, the scope and novelty of the current study is:

1. Structural applications of GNPs in cement composites in concrete structures subjected to extreme dry shrinkage, flexural bending, and impact loading.
2. Development of optimum GNPs cement composites for strengthening, retrofitting, and cracks repairing purposes of damaged concrete structures.
3. State of art solution to provide real time micro-cracking monitoring and damage evaluation of GNPs-cement composites in concrete constructions under AE technology.

2. Analyses methods

2.1. b-value method

The b-value analysis approach was initially implemented in seismic wave studies, and since then, it has gained widespread acceptance among seismologists to assess seismicity [40]. Such method can also study the AE research area because acoustic waves are comparable to seismic waves produced during AE events. The b-value method for AE analysis can be determined using the Gutenberg-Richter (GR) [41] equation of seismicity, as follows in Eq. (1) [42]:

$$\log_{10}N = \mathrm{a} - \mathrm{b}\left(\frac{A_{dB}}{20}\right) \tag{1}$$

Where N is the number of AE events with magnitudes greater than A_{dB}, A_{dB} is the peak AE amplitude, a is the intercept along the $\log_{10}N - axis$, and b is the slope of base ten loglines plotted against A_{dB}. Eq. (1) indicates that the b-value increases with the initiation of micro-cracks. In contrast, the b-value decreases after the formation of macro-cracks. To explain the statistical values of AE events, the improved b-value (Ib-value) analytical technique was developed by T. Shiotani et al. [30] which can be appropriately used for concrete and geotechnical materials, calculated as follows in Eq. (2):

$$\mathrm{Ib} = \frac{\log_{10}\mathrm{N}(\mu - \alpha_1\sigma) + (\mu + \alpha_2\sigma)}{(\alpha_1 + \alpha_2)\sigma} \tag{2}$$

Where σ and μ are the standard deviation and mean values of AE events, respectively; α_1 and α_2 are the coefficients related to the AE amplitude, ranging from − 1–1. Every new hit recorded throughout the fracturing process updates the Ib-value considered a transient feature. The parameter N is often set to the closest 100 hits ($N = 100$) since the Ib-value is so sensitive, it can monitor minor fracture occurrences [43].

2.2. Average frequency (AF) versus RA value analysis

In cement composites, tensile and shear cracks are two predominant types of cracks. The process of failure begins with the formation of many microscopic tensile fractures. As the strain on the material increases, the tiny tensile cracks join with each other and eventually grow into macroscopic shear cracks [44]. The average frequency (AF) is defined as the ratio of ringdown counts to the duration, whereas; RA is defined as the ratio of rise time to the amplitude, measured in μs/V. Based on the following Eqs. (3) and (4), the two parameters can be calculated as:

$$\mathrm{AF} = \frac{\text{ringdown counts}}{\text{duration}} \tag{3}$$

$$\mathrm{RA} = \frac{\text{rise time}}{\text{amplitude}} \tag{4}$$

The existing literature [23] shows that tensile fracture corresponds to an AE signal with low RA value and high AF, while shear fracture corresponds to an AE signal with high RA value and low AF.

2.3. AE intensity analysis

The trend of AE data is determined by the intensity of the AE signal based on the consideration of the amplitude and duration, and can be used to evaluate the deterioration and the general integrity of the specimen [37]. The plot of the historical index $(HI)$and severity index $\left(\log_{10}S_r\right)$, used in crack intensity analysis were both dependent on the AE signal strength [45]. The Historical Index (HI) is an analytical approach for comparing the signal strength of the most recent AE event to all AE occurrences [46]. It is derived using the following Eq. (5):

$$\mathrm{HI(t)} = \frac{\mathrm{N}}{\mathrm{N} - \mathrm{K}} \frac{\sum_{\mathrm{i=K+1}}^{\mathrm{N}} \mathrm{S_{oi}}}{\sum_{\mathrm{i=1}}^{\mathrm{N}} \mathrm{S_{oi}}} \tag{5}$$

Where N represents the cumulative number of hits until the time (t); S_{oi} represents the signal strength of i^{th} AE hit, and K represents an

Table 1
K-parameter for concrete structure [23].

No. of hits (N)	≤ 50	51–200	201–500	≥ 501
K	Not applicable	N-30	0.85 N	N-75

empirical material constant, as shown in Table 1.

The average signal strength for the fifty AE hits with the highest numerical value of peak amplitudes is known as the severity(S_r) [37]. It is calculable as follows in Eq. (6):

$$S_r = \frac{1}{J}\sum_{i=1}^{J} S_{oi} \tag{6}$$

where $S_r$represents the severity index,S_{oi} is the i^{th}-largest signal strength, and J represents the empirical constant for concrete, as shown in Table 2.

3. Materials and experimental program

3.1. Materials and mixed proportions

The materials for casting GNPs-cement composites were comprised of tap water, P.O.42.5 Portland cement, and GNPs used in the mechanical testing. GNPs used in this research came from the Times nano Web (Chengdu, China). A surfactant, Acacia Gum (AG-natural polysaccharide), was utilized as per the recommendations of previous related research to disperse and improve the workability of the nano-modified GNPs cementitious composites [47]. Acacia Gum (average particle size of 205 μm, viscosity 70–110mm^2/s, PH: 5.0) was purchased from Kemiou chemical reagent Co. Ltd (Tianjin, China).Tables 3 and 4 illustrate the physical properties of cement, as well as the key properties of the GNPs. A total of 3 formulations, with graphene contents of 0 wt%, 0.04 wt%, and 0.08 wt% over cement weight were prepared and tested to measure the response of nanoplatelets presence on the fracture and mechanical performance of cement composites. The three-point bending followed by compression test was performed on a total of 54 specimens, with 18 specimens of each formulation being fabricated. In each formulation, the water to cement ratio was maintained at 0.35, and a graphene-to-surfactant ratio of 1:1 was used for this research. The process of fresh and mechanical testing of the GNPs-cement composites was characterized as the "mixing, vibrating, and curing" method (ISO Method) (GB/T 17671–1991). The specific mix proportions of the GNPs-cement composites formulations and the specimen designations are summarized in Table 5.

3.2. Specimen preparation

Fig. 1 represents the schematic plan for the preparation of GNPs-cement composites. To produce a homogenous aqueous solution of acacia gum, individual 0.04 wt%, and 0.08 wt% acacia gum by weight of cement binder was added to the water and then agitated for 15 min. Then, as shown in Table 5, GNPs were added to the aqueous solution in the proportions of (0.04 wt% and 0.08 wt%) by weight of cement. Afterward, a probe ultrasonicator (operated at 100 W at the speed of 3000 rpm) was used to thoroughly mix the GNPs suspensions for 30 and 60 min, respectively. During the whole sonication process, the vessel containing the GNPs suspensions was submerged in cold water to maintain a low temperature in the solution. Additionally, the beaker was covered with a plastic sheet to prevent water from evaporating.

In the next step, the ultrasonic treated GNPs suspensions were mixed with ordinary Portland cement using an agitator kettle. They were treated through a multispeed planetary mixer for a total of 5 min, at low and high speeds successively. In the final step, the mixture was poured into 40 mm × 40 mm × 160 mm size oiled steel moulds immediately and shaken them for 1 min at the vibrating table to eliminate the air bubbles. Before demolding, all specimens were maintained at room temperature in the laboratory. The specimens were weighed, labelled, and then placed in a 100% humidity environment for 28 days of curing after they were demolded (24 h later).

3.3. Physical properties

3.3.1. UV–vis spectroscopy of GNPs aqueous solution

The degree of dispersion was measured using (UV–vis) in the presence of surfactant to analyse the dispersion results [48]. The Beer-Lambert law was used to monitor and demonstrate their absorbency. According to Lambert-Beer's law: $A = \log\frac{1}{T} = \log\frac{I_r}{I_s} = E\,Cl$, the strength of the dispersed solution is linear to the absorbency of solution in a certain wavelength; where A=absorbance, T = light transmittance, I_r= intensity of incident radiation, I_s=intensity of transmitted radiation, E = molar absorption coefficient, C=solution concentration, and l=optical path length. According to previous research, a peak of absorption at 270 nm was seen in the UV–vis absorption spectra of graphene. This peak is usually primarily caused by the agitation of the π-Plasmon dispersion relation of AA-stacked graphite [49].

Table 2
J value for concrete structures [23].

No. of hits (*N*)	<50	≥ 50
J	Not applicable	50

Table 3
Physical properties of reference cement.

Density [g/cm^3]	Specific surface area[m^2/kg]	Consistency [%]	Setting time (min)		Compressive strength [MPa]		Flexural strength [MPa]	
			Initial	Final	3d	28d	3d	28d
3	352	26	159	235	30.0	55.2	5.9	8.3

Table 4
Properties of graphene nanoplatelets.

Diameter [μm]	Thickness [nm]	Purity [%]	Layers	PH value	Specific surface area [m^2/g]	Bulk density [g/cm^3]
5–10	4–20	> 99.5%	< 20	7.0–7.5	> 750	0.6

Table 5
Mix design of modified GNPs cement composites specimens.

Formulation ID	W/C	GNPs Amount (%)	Acacia Gum (%)
GNP-0	0.35	-	-
GNP-4	0.35	0.04	0.04
GNP-8	0.35	0.08	0.08

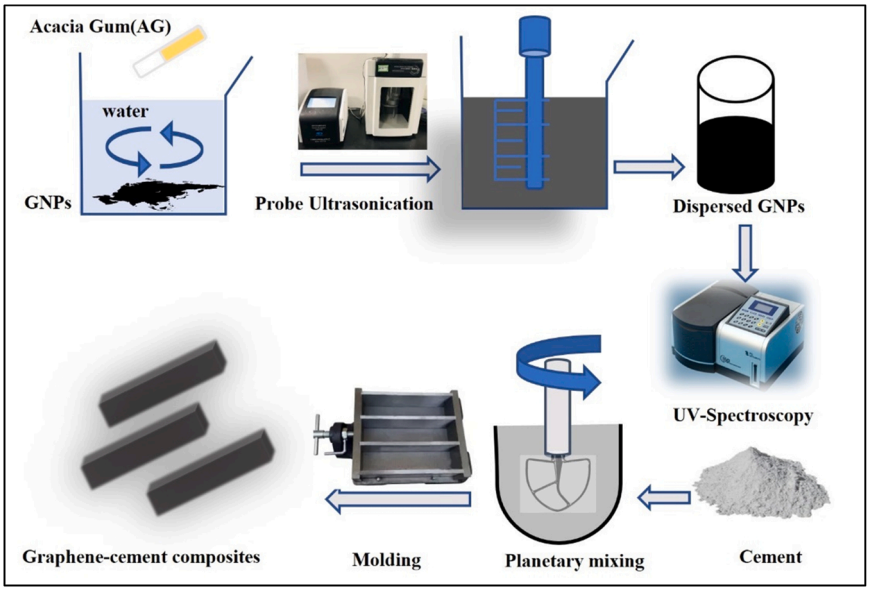

Fig. 1. Preparation of dispersed solution and casting produce of GNPs-cement composites specimens.

3.3.2. Scanning electron microscopy

The microstructure, surface texture, and morphology study of GNPs in cement matrix were examined using a Field Emission Scanning Electron Microscope (FESEM) Nova Nano SEM 450, FEI Co. on fractured cement fragments(1 cm × 1 cm). During mechanical testing, they were collected from fragments of broken representative formulations, and ethanol was used to inhibit further hydration.

3.4. Apparatus and experimental methods

3.4.1. AE test

Fig. 2 depicts the test apparatus for AE monitoring based on the three-point bending test. For fractures monitoring, the sensor R6α was mounted onto the specimens with an operating frequency range of about 35–100 kHz. The AE response was recorded using Micro-II Digital AE System (provided by Physical Acoustic Corporation) and AE^{win} software. In this test, the AE signal was amplified by 40 dB, as most of the AE signals are very weak and need preamplifier for amplification. The acquisition threshold was set at 40 dB to maintain

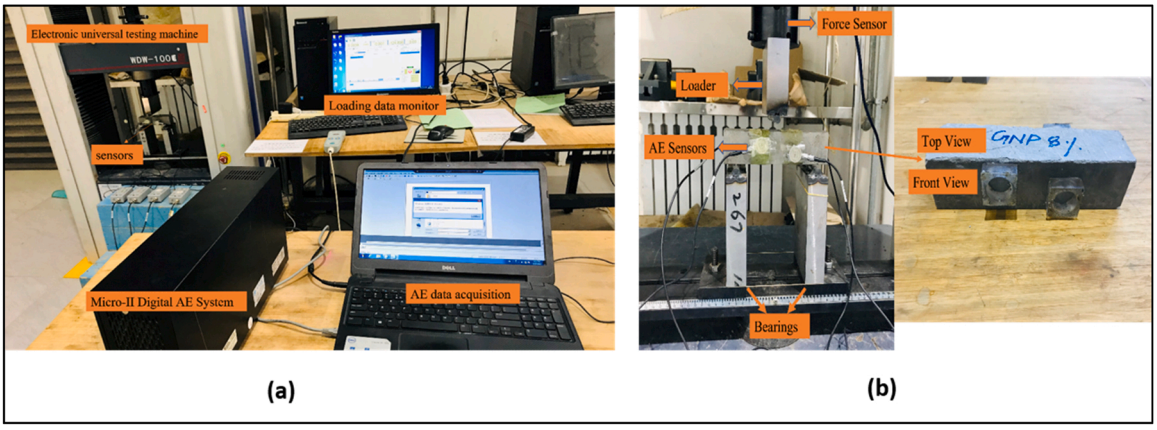

Fig. 2. (a) Experimental setup for three-point bending test mounted with AE monitoring of GNPs-cement matrix; (b) Sensors configuration and details views of GNPs-cement composites specimen.

a good signal-to-noise ratio. As shown in Fig. 3, a typical AE waveform can be determined from key parameters such as amplitude, duration, counts, energy, and rise time.

The span length, the distance between the two lower supports, equals 100 mm. The GNP-cement composites were tested in a universal testing machine (WDE-100E) by employing static load at a strain rate of 0.05 mm/min. The four sensor centres were spaced 15 mm, 25 mm, 15 mm, and 25 mm apart from the specimen top corner, as shown in Fig. 4. These sensors were positioned 55 mm, 105 mm, 55 mm, and 105 mm apart from the left corner, respectively. As showed in Fig. 2(b), silicon grease was used as a coupling agent to attach the four sensors to the specimen surfaces.

3.4.2. Test method for compressive strength

Refer to GB/T17671–1999 "Cement paste strength test method (ISO method)," the compressive strength of GNP-cement composites was tested after 3, 7, and 28 days of curing. A 2400 N/s + 200 N/s loading rate was used for operating the testing equipment (WHY-300) to determine the compressive strength of each fractured piece. The test results were calculated using the average value of six specimens, unless > + 10% of the average specimens.

4. Results and discussion

4.1. Dispersion of GNPs suspensions

The strong Wan der Waals forces and large surface areas of the particles are the main issues with the dispersion of GNPs. Additionally, the individual sheets in GNPs exhibit a π-π bond, which causes stacking. Thus, adding a surfactant (Acacia Gum) can significantly help to break these strong interparticle interactions and reduce these strong attractions, allowing for homogeneous GNPs

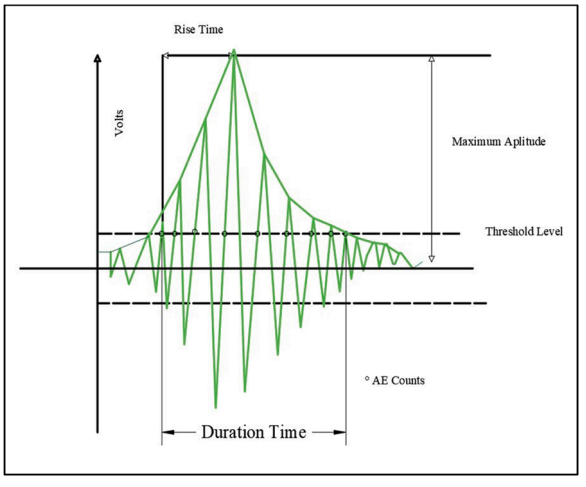

Fig. 3. Typical AE signal.

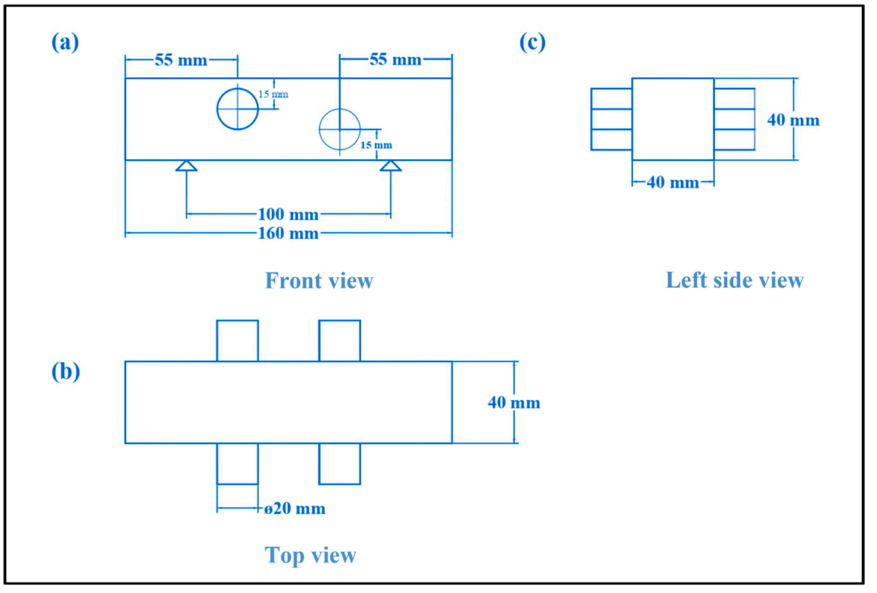

Fig. 4. Typical illustrations of AE sensors placement and geometry of GNPs-cement matrix.

dispersion. The UV–vis results for GNPs suspensions at 30-minute and one-hour sonication durations is shown in Fig. 5 regarding the absorbance value at 200–900 nm wavelength. Results indicated that introducing acacia gum while using sonication energy produces well-dispersed aqueous solutions. As demonstrated in Fig. 5, there was a direct relationship found between the absorbance of GNPs contents and sonication period as illustrated in Xu et al. [36]. The UV–vis absorption spectra of the 0.04 wt% and 0.08 wt% graphene concentrations showed the largest peak of the absorption wavelength at 267 nm. As shown in Fig. 5(b), when the sonication period was extended from 30 to 60 min, the GNP-4 showed better dispersion than GNP-8. Due to the larger size and weight of GNPs, which need more energy to disperse [47], the GNP-8 absorbance value was lower than that of GNP-4. The absorption value of GNPs suspensions ceased to rise after 60 min of sonication, regardless of the sonication period.

4.2. *Mechanical properties*

The load-deflection curves obtained during the three-point bending test at 28 days of curing of reference and specimens reinforced with the addition of GNPs are shown in Fig. 6. The entire GNPs- cement composites exhibited in three distinct mechanical stages against the three-point bending loading i.e., (1) Stage I; pre-peak: (2) stage II; peak: (3) stage III; post-peak. The addition of GNPs in the reference specimens significantly improved the post-peak response. Also, the GNPs- cement composites exhibited steep slope

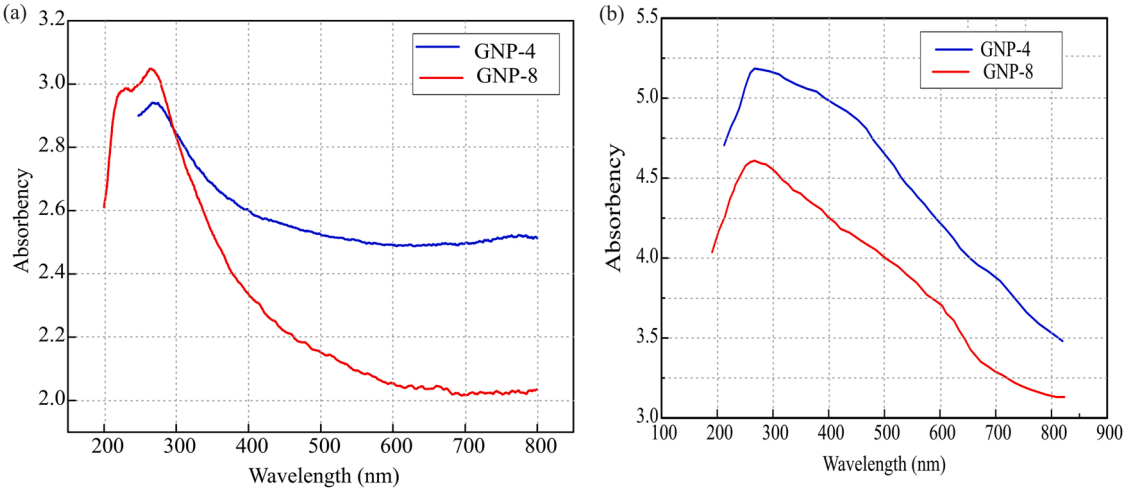

Fig. 5. UV-Vis spectrum of 0.04 wt% and 0.08 wt% over cement weight GNPs-suspension as a function of sonication time: (a) after 30 min sonication; (b)after 1 hr. sonication.

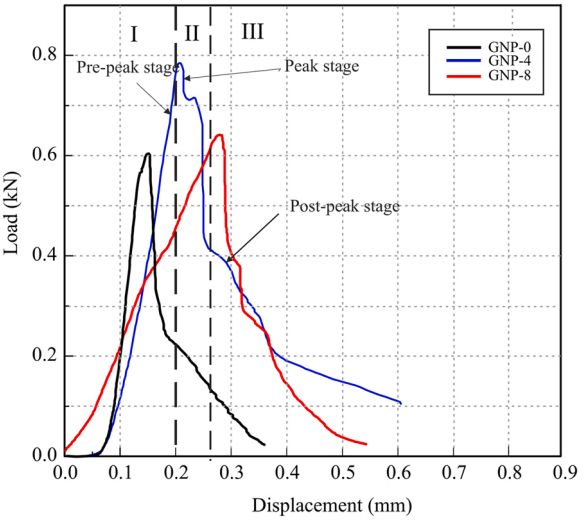

Fig. 6. Typical load-deflection curves of GNPs-cement composite specimens; GNP-0, GNP-4 and GNP-8.

behaviour during the first two stages leading to the facts that the specimens have higher bending stiffness against applied load and can be more suitable for cracks repairing and retrofitting purposes of damaged concrete structures. It was observed that cement composites reinforced with GNPs need larger stress to obtain the same deflection than GNP-0. This can be concluded that nano reinforcements play a vital role in nano/micro size crack inhibition as well as in increasing load-bearing capacity of concrete structures [17].

Compressive and flexural strengths of GNPs- cement composites at different ages were showed in Fig. 7. In comparison to the reference specimen (GNP-0), the GNP-4 formulation showed excellent performance, with flexural strength and compressive strength reaching 9.6 MPa, 10.5 MPa, 12.4 MPa, and 40.1 MPa, 47.5 MPa, 62.5 MPa at 3, 7, and 28 days of age, respectively, with an increase in flexural strength of 26.3%, 29.62%, 34.7%, and an increase in compressive strength of 11.3%, 11.7%, 13.4%, respectively. On the other hand, in GNP-8 formulation, the flexural strength and compressive strength reached 8.6 MPa, 9.2 MPa, 10.2 MPa, and 38 MPa, 45 MPa,57 MPa, after cured 3d,7d and 28d, respectively, with the amplification of 13.1%,13.5%,10.8% and 5.5%,5.8%,3.4% in flexural and compressive strength compared to reference specimen. Based on the obtained results, a well-dispersed GNPs in cement composites enhances compressive and flexural strength while resulting in more excellent energy absorption during final failure against the extreme loading.

4.3. Micro- and macro-crack detection by acoustic emission analysis

The fluctuations of numerous AE parameters computed during the three-point bending test were associated with three distinct phases of damage progression to determine micro- and macro cracking.

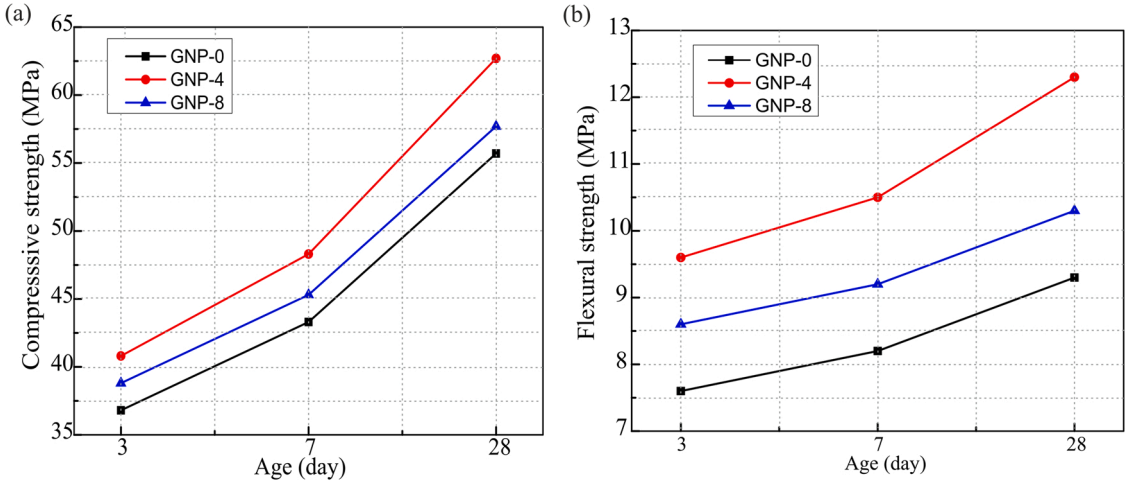

Fig. 7. Mechanical characteristics: (a) Compressive strength of GNPs-cement composites; and (b) Flexural strength of GNPs-cement composites.

4.3.1. Cumulative number of hits and cumulative energy

The AE parameter curves of the three alternative formulations are depicted in Fig. 8, and it can be observed that the accumulated energy and the cumulative number of hits trends are the same. The entire microcracking response of the tested specimens comprised of three main stages as reported by Xue et al. [36]. In stage (I); the AE activities of the GNP-4 and GNP-8 were analogous to those of the GNP-0 with 30000 and 7500 cumulative energies. Stage (II) was the strengthening stage, where all the specimens exhibited a peak response; stage (III) was the failure stage, GNP-4 and GNP-8 exhibited more AE activity of 5200 and 4700 hits due to the high strain fracture mechanism than that of GNP-0 which was 4150 hits. The load-time and AE hits of the GNP-4 and GNP-8 formulations varied slightly. Despite initiating slowly, the GNP-4 and GNP-8 formulations exhibited considerable increment as the stress increased. GNP-8 formulation contained more fractures in the first stage due to the larger size and weight of GNPs particles, which resulted in an inevitable accumulation of damage in early stage of loading.

In addition, the cumulative energy of the AE hits gradually increased initially, but after the load exceeded the maximum limit (>60%), AE cumulative energy raised substantially. The GNP-0 possessed a significant amount of energy before the peak stress. However, the cracks started growing as the peak stress reached to its limit and thus, the generation of macrocracks eventually formed a fracture zone. In stage (I), the AE energy of the GNP-4 formulation was low, fractures were minor, and there was no significant cracking prior to fracture unlike in the GNP-0 which demonstrated that GNP-4 has high fracture toughness.

4.3.2. Amplitude distribution

As showed in Fig. 9(a), the amplitude distribution range in the GNP-0 lies between 40 and 60 dB during stage I. However, the amount of AE activities in a total duration of 60–110 s were maximum during the peak stage (II), which clearly indicates that microcracking activities were at a peak at this stage. A gradual decrease was observed in recorded AE amplitude during the last (III) fracture stage that comes soon after the specimens reached their peak response in terms of load-displacement behaviour.

Similarly, as showed in Fig. 9(b-c); the recorded AE amplitude in GNP-4 and GNP-8 formulations touched a maximum limit of 70 and 80-dB during stage (II), corresponding to the maximum duration limit of 60–170 and 45–180 s, respectively. Thus, these experimental observations can be explained that less AE activities generated once the intensity of the growth rate of cracking becomes higher, corresponding to the time duration of AE signals. In addition, the mechanical performance of different GNPs-cement composites also greatly varied with the addition of GNPs in reference cement composites bringing the denser distribution of AE amplitude

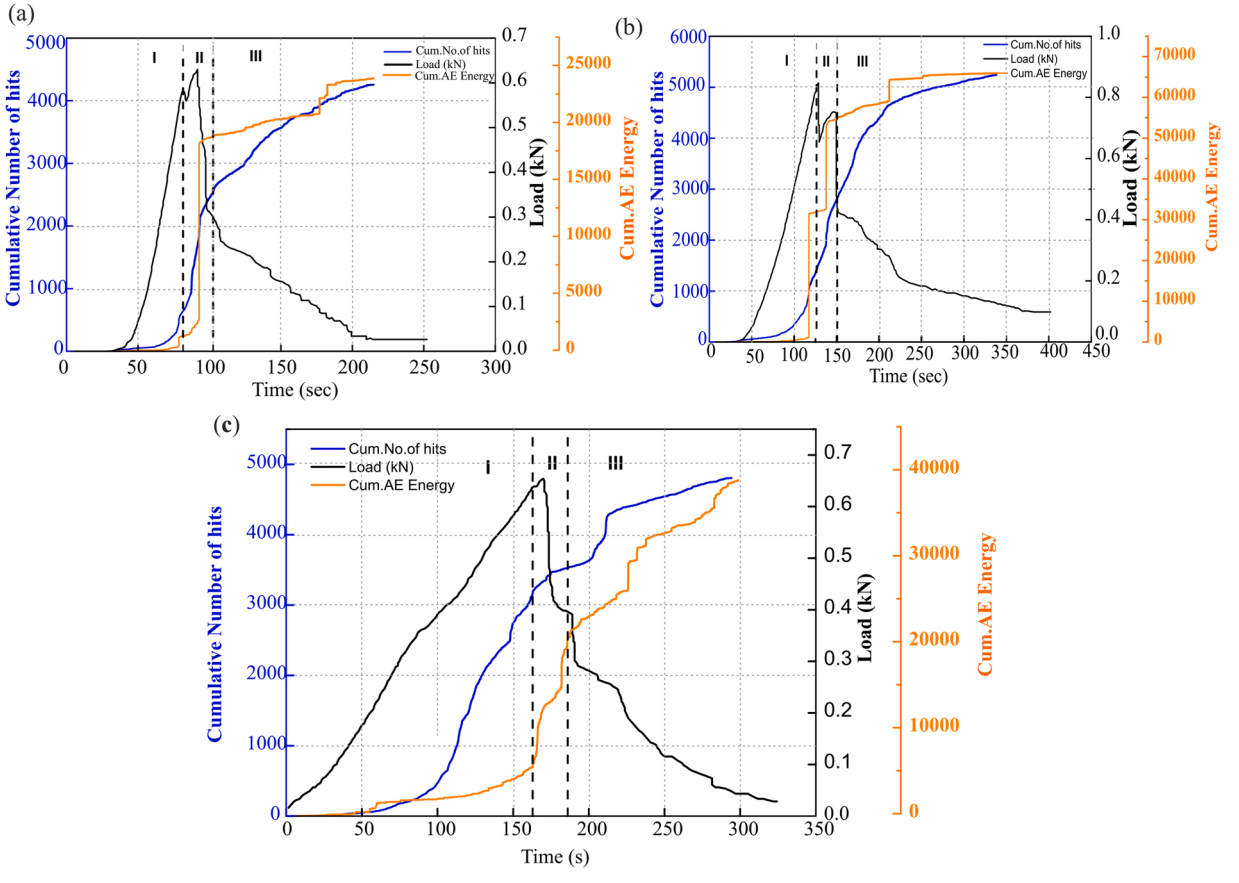

Fig. 8. AE cumulative number of hits and cumulative energy: (a) (GNP-0); (b) GNP-4; and (c)GNP-8.

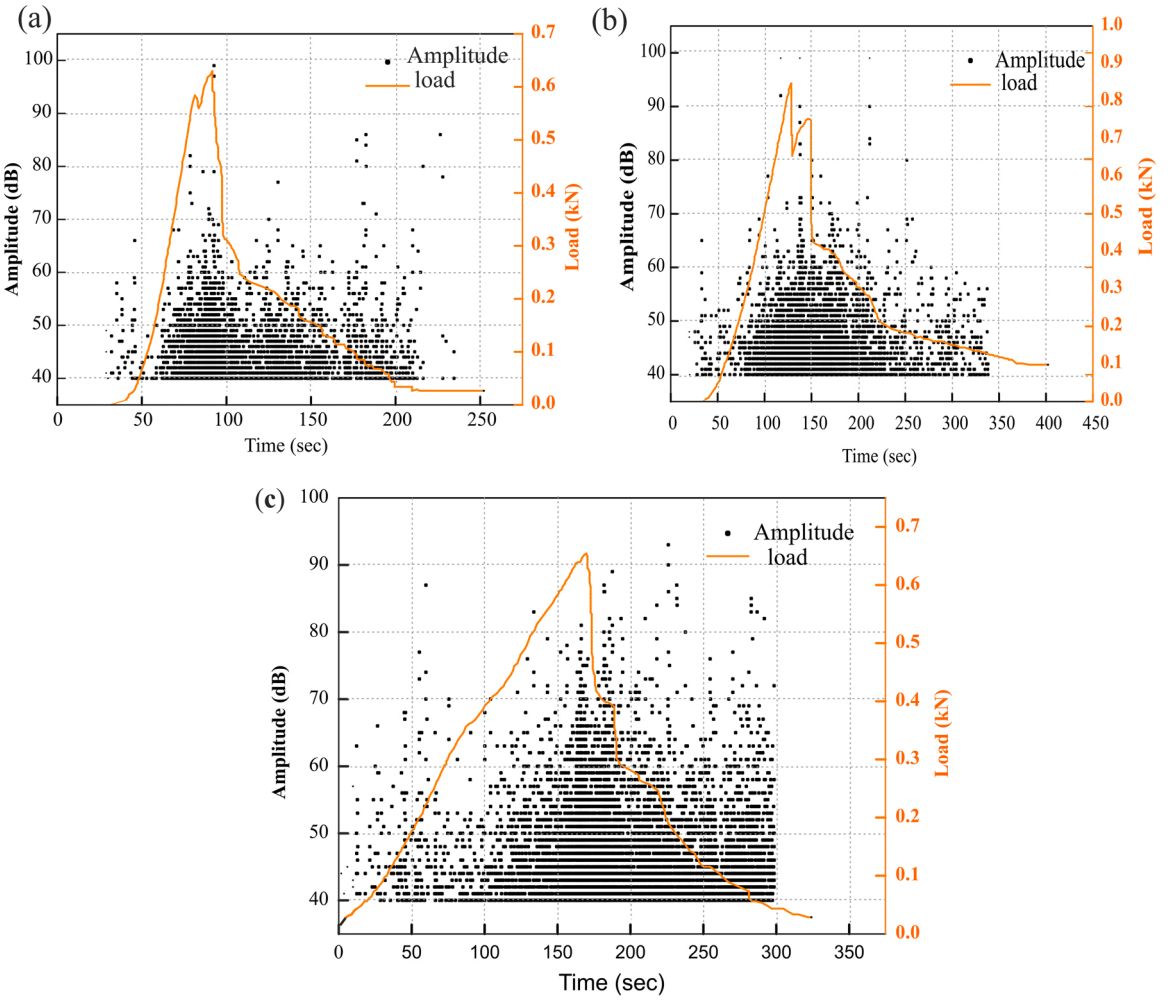

Fig. 9. AE amplitude distribution: (a) GNP-0; (b) GNP-4; and (c) GNP-8.

across the nano-reinforced GNPs tested specimens due to their strong damping and ductility. Consequently, such phenomenon increased the AE energy due to excessive micro-cracking activities. Furthermore, the strength of AE signals became weak in terms of AE amplitude because of the micro-cracks leading toward macro-cracks; thus, the attached sensors couldn't detect low AE signals during the macro-cracking behaviour of the tested specimens. Overall, the damping capacity and ductility of GNP-4 was improved by 25.1% and 22.47% compared to the GNP-0.

4.3.3. RA-AF value

High RA values at 40000 μs/V in three-point bending tests indicate a shear fracture, whereas low RA values near 20000 μs/V indicate tensile fracture mode [50]. In similar way, the lower AF value (>35 kHz) of concrete structures suggests shear failure, while higher AF value (<35 kHz) results in tensile failure [51]. A distinct shear failure mode was characterized through a range of RA values between 31000 μs/V for the GNP-0, as showed in Fig. 10. In contrast, a significant tensile failure was indicated by a range of RA values between 20000 μs/V for the GNP-4 and GNP-8 formulations, respectively. As a result, the cracking mechanism in the GNP-0 changed from shear failure to tensile failure with the incorporation of graphene nanoplatelets. The RA value distribution of the GNP-0 was wider and showed a more significant upwards progression while examining the RA-AF distributions of the three different formulations, which corresponds to a higher degree of damage. The RA value distribution of GNP-4 was smaller and with less upward movement, corresponding to a lower degree of damage and better integrity. In contrast, the RA value distribution of GNPs-8 was spaced between that of GNP-0 and GNP-4. Based on AF analysis, the GNP-4 and GNP-8 showed tensile failure with AF values of 0–200 kHz and 0–300 kHz compared to the GNP-0 which 0–35 kHz.

4.3.4. Ib-value

The Ib-value was calculated using 100 recent hits that were recorded during the fracture process. As showed in Fig. 11, the trends of the Ib-values of the three formulations were similar below the warning Ib value of 1.5. Fig. 11(a), represents the cracking pattern of

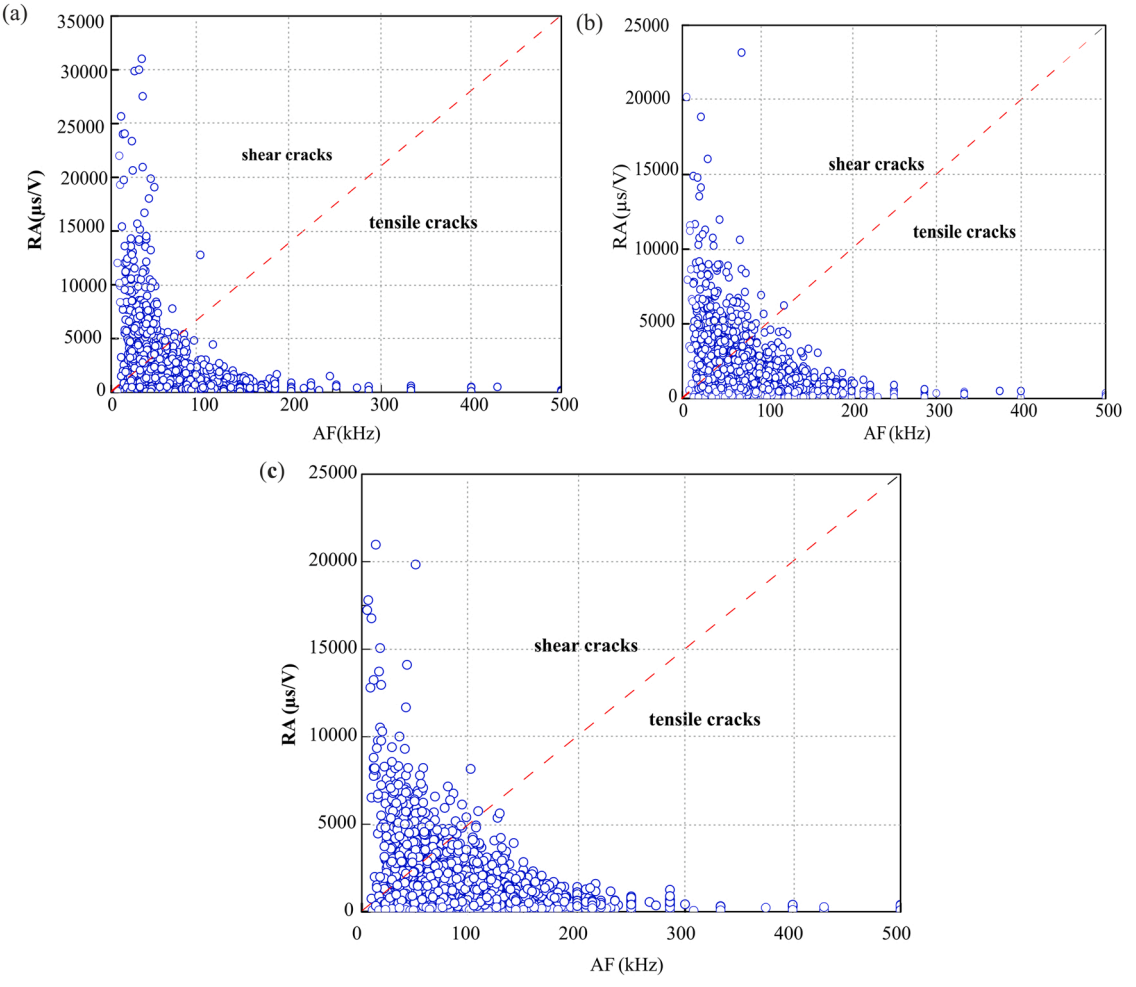

Fig. 10. The RA-AF value of: (a) GNP-0; (b) GNP-4; and (c) GNP-8.

GNP-0 attributed to Ib-values, which were increased early in the development of microcracks, indicating that the damage in the GNP-0 was homogeneous and minor. However, the Ib-values were declined dramatically around the peak load point, indicating the generation of macrocracks. In the loading stage, the Ib-values of GNP-4 were low, indicating that microcracks were formed in the fracture process zones. Hence, the degree of damage was lower than that of the GNP-0. The crack formation of GNP-8 was minor and developed slowly in the initial stage because the Ib-values fluctuation range was smaller, with a slight drop prior to attaining the ultimate load. During the main collapsed stage, a significant declined trend, as showed in Fig. 11(a-c), was observed in Ib-value in all tested specimens indicating a clear transfer of micro into macro-cracks failure mode.

4.3.5. AE intensity analysis

The HI curves for the GNP-0, GNP-4, and GNP-8 specimens are shown in Fig. 12(a). A substantial deterioration was begun to occur in the cement composites as the HI curve reached its peak. A high peak in the loading stage of the control specimens shows considerable damage. There was no peak in the initial loading stage of the GNP-4 HI curve, indicating that the damage to the cement composite material was minor and the mechanical performance was good. However, at a later stage of loading, there was a high peak value of acoustic emission intensity which resulted in failure of GNP-4, corresponding to cement hydration and strong bonds between products in graphene. Fig. 12(b), shows the Sr-time relationships of the GNP-0, GNP-4, and GNP-8 specimens. Slope changes in the Sr-time curve indicated the presence of new major cracks in the AE signals. There were several sharp peaks in the acoustic emission signal of the GNP-0 during the loading process. On the other hand, the GNP-4 showed a stable and smooth curve, including high mechanical performance throughout the three-point bending loading.

The damage assessment of GNPs-cement composites was determined through HI vs. lg Sr plot. Fig. 12(c), displays the analysis of AE signal strength using HI vs. lg Sr factors. The severity of the damage associated with the AE signal source increased when the point was moved away from the upper right corner. The closer the point is to the bottom left corner, the less influence it has on the source of the acoustic emission signal. HI and Sr values higher than the normal range indicates that the cementitious materials are potentially in the harmful stage. Fig. 12(c), depicts the suggested limit for the GNP-0 safe region, as lgSr = 5 and HI = 2.5. The presence of GNPs boosts

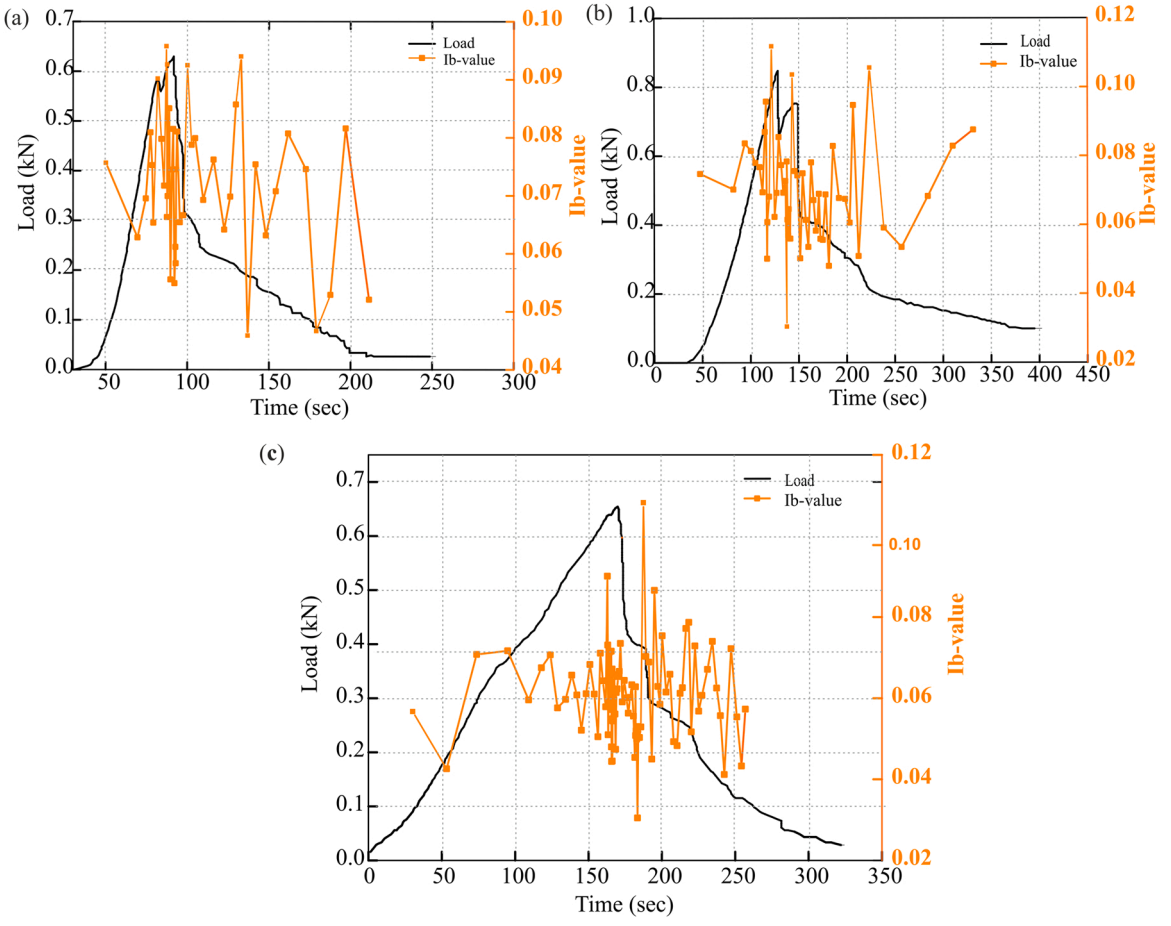

Fig. 11. Ib-value analysis of: (a) GNP-0; (b) GNP-4; and (c) GNP-8.

the cement composites safety reserves, as shown by the HI value for GNP-4, which was 3–4 times greater than the normal value.

4.4. Microstructure characterization of GNPs-cement composites

The microstructure comparison between the plain cement pastes and GNP-cement composites was depicted in Fig. 13. As illustrated in Fig. 13(a), the plain cement paste had a severe crack of 1.44 mm that passed directly across the whole hydration of the cement product. On the other hand, as showed in Fig. 13(b-d), there were no apparent cracks, and adding GNPs into cement composites enhanced the abundance of cement hydrates. The addition of GNPs into a cement composite resulted in a layered structure that was denser and less porous and organized in layering assembly. It implies that GNPs could function in altering the form of cement hydrated products and filling the cement-composite structures pores and cracks, which prevents crack propagation under the external load. It can be seen from Fig. 13(d), that the sheet-like aggregates were observed when the GNPs content increased to 0.08 wt% in the cement matrix. It was hypothesized that the accumulation of GNPs particles may have produced this behaviour in the cement matrix. Because of the high concentration of GNPs in the cement matrix, it is possible that they will form a blockage and will not combine with the surrounding cement matrix. As a result, the density of the structure will be reduced, and the mechanical properties of the cement composite will be decreased.

5. Conclusions

The present study employed the AE technique to monitor the crack propagation and damage evaluation of GNPs-cement composite specimens with reinforcement ratios of (0 wt%,0.04 wt%, and 0.08 wt%) over the weight of cement, respectively. Four AE sensors continuously collected the AE signals released under the three-point bending test. The collected AE data were analyzed by AE parameters such as the cumulative number of hits, cumulative energy, amplitude distributions, and three representative analyses methods, including the RA vs. AF, Ib-value method, and signal intensity analysis to reveal the cracking characteristics and damage process of GNPs-cement composites. The following were the main conclusions that may be drawn:

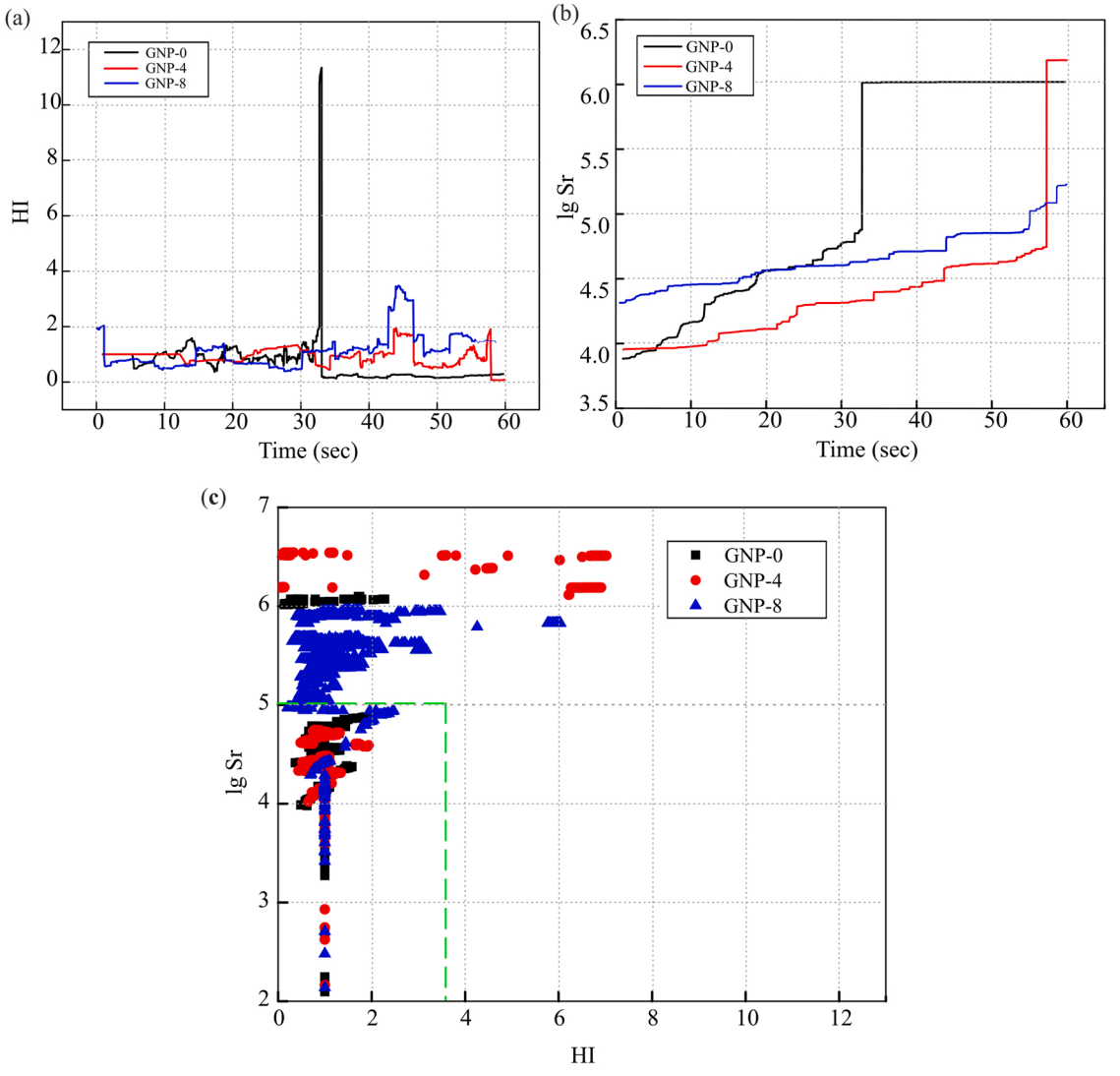

Fig. 12. AE intensity analysis: (a) HI curves; (b) lg Sr curves; and (c) Plot of HI vs. lg Sr.

1. As evident through UV–vis results and SEM images, the dosage of GNPs at 0.04 wt% by weight of cement binder showed a maximum absorbency rate at 60 min sonication period, which proved to be an excellent dispersion agent in cement composite.
2. The GNPs-cement composites showed mechanical performance in three distinct stages under mechanical degradation: namely, initial stage (I), pre-peak stage (II), and post-peak stage (III).
3. The compressive and flexural strengths of GNP-4 was improved by 12.71% and 30%, respectively, compared to the GNP-0.
4. Based on the analysis of the AE parameters, the results of GNPs-cement composites obtained from the three-point bending test precisely detected micro- and macro-cracks at the early-stage loading. The GNP-4 specimen exhibited higher hits activity, cumulative energy, HI(t), and Sr, and a lower Ib-value than the GNP-0, which was attributable to higher compressive and flexural strengths.
5. The GNPs in cement composites caused a bridging effect among graphene-cement particles, which prevented the development of cracks during the early stages of loading.
6. The GNP-4 and GNP-8 exhibited tensile fractures, while GNP-0 resulted brittle fractures.
7. The safety reserve and cracks assessment through signal intensity analysis with a safe limit of HI = 2.2 and lgSr = 5 was identified in a pattern of GNPs-4 >GNPs-8 >GNP-0. The results revealed that the cement composites combined with GNPs possessed a more significant damage safety margin than the reference specimens.

CRediT authorship contribution statement

Shahzad Ashraf: Conceptualization, Methodology, Experimental investigation, Formal analysis, Writing – original draft,

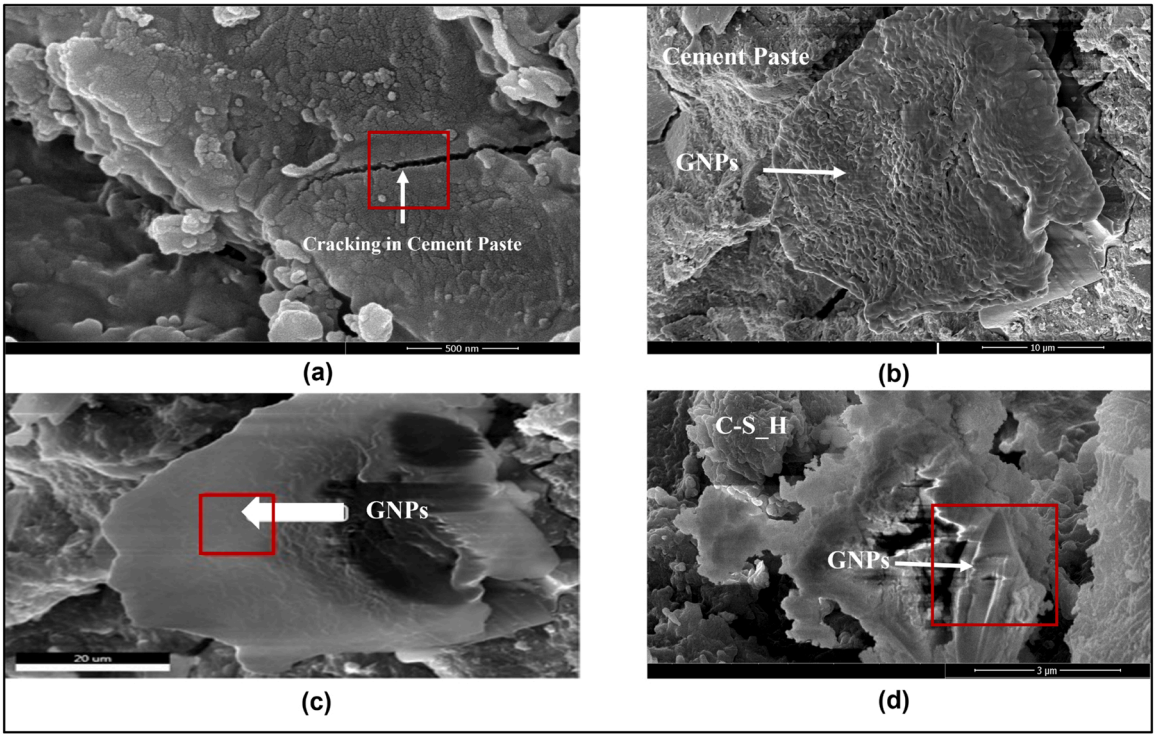

Fig. 13. (a) SEM image of reference matrix; (b) GNPs-hydrated products of cement matrix;(c) 0.04 wt% over cement weight GNPs embedded in cement matrix (d) 0.08 wt% over cement weight GNPs embedded in cement matrix.

Visualisation, Supervision. **Suliman Khan**: Formal analysis, Visualisation, Writing – review & editing. **Vipin Kumar Oad**: Formal analysis, Visualisation, Review.

Declaration of Competing Interest

The authors declare that they have no known competing financial interests or personal relationships that could have appeared to influence the work reported in this paper.

Data availability

Data will be made available on request.

References

[1] D.Y. Yoo, Y.S. Yoon, A review on structural behavior, design, and application of ultra-high-performance fiber-reinforced concrete, Int J. Concr. Struct. Mater. 10 (2016) 125–142, https://doi.org/10.1007/s40069-016-0143-x.
[2] S. Ghourchian, M. Wyrzykowski, P. Lura, A practical approach for reducing the risk of plastic shrinkage cracking of concrete, RILEM Tech. Lett. 2 (2017) 40–44, https://doi.org/10.21809/rilemtechlett.2017.45.
[3] M. Safiuddin, A.B.M.A. Kaish, C.O. Woon, S.N. Raman, Early-age cracking in concrete: causes, consequences, remedialmeasures, and recommendations, Appl. Sci. (Switz.) 8 (2018), https://doi.org/10.3390/app8101730.
[4] V. Marcos-Meson, A. Michel, A. Solgaard, G. Fischer, C. Edvardsen, T.L. Skovhus, Corrosion resistance of steel fibre reinforced concrete - A literature review, Cem. Concr. Res 103 (2018) 1–20, https://doi.org/10.1016/j.cemconres.2017.05.016.
[5] Y. Ding, Z. Chen, Z. Han, Y. Zhang, F. Pacheco-Torgal, Nano-carbon black and carbon fiber as conductive materials for the diagnosing of the damage of concrete beam, Constr. Build. Mater. 43 (2013) 233–241, https://doi.org/10.1016/j.conbuildmat.2013.02.010.
[6] K.M. Liew, Z. Pan, L.W. Zhang, The recent progress of functionally graded CNT reinforced composites and structures, Sci. China Phys. Mech. Astron 63 (2020), https://doi.org/10.1007/s11433-019-1457-2.
[7] V.D. Ho, C.T. Ng, C.J. Coghlan, A. Goodwin, C. Mc Guckin, T. Ozbakkaloglu, D. Losic, Electrochemically produced graphene with ultra large particles enhances mechanical properties of Portland cement mortar, Constr. Build. Mater. 234 (2020), https://doi.org/10.1016/j.conbuildmat.2019.117403.
[8] K. Snehal, B.B. Das, M. Akanksha, Early age, hydration, mechanical and microstructure properties of nano-silica blended cementitious composites, Constr. Build. Mater. 233 (2020), https://doi.org/10.1016/j.conbuildmat.2019.117212.
[9] I. Dejaeghere, M. Sonebi, G. de Schutter, Influence of nano-clay on rheology, fresh properties, heat of hydration and strength of cement-based mortars, Constr. Build. Mater. 222 (2019) 73–85, https://doi.org/10.1016/j.conbuildmat.2019.06.111.
[10] Atta-ur-Rehman, J.H. Kim, H.G. Kim, A. Qudoos, J.S. Ryou, Effect of leaching on the hardened, microstructural and self-cleaning characteristics of titanium dioxide containing cement mortars, Constr. Build. Mater. 207 (2019) 640–650, https://doi.org/10.1016/j.conbuildmat.2019.02.170.
[11] A.A. Balandin, S. Ghosh, W. Bao, I. Calizo, D. Teweldebrhan, F. Miao, C.N. Lau, Superior thermal conductivity of single-layer graphene, Nano Lett. 8 (2008) 902–907, https://doi.org/10.1021/nl0731872.

[12] J.L. Le, H. Du, S.D. Pang, Use of 2-D graphene nanoplatelets (GNP) in cement composites for structural health evaluation, Compos B Eng. 67 (2014) 555–563, https://doi.org/10.1016/j.compositesb.2014.08.005.
[13] B. Han, Q. Zheng, S. Sun, S. Dong, L. Zhang, X. Yu, J. Ou, Enhancing mechanisms of multi-layer graphenes to cementitious composites, Compos Part A Appl. Sci. Manuf. 101 (2017) 143–150, https://doi.org/10.1016/j.compositesa.2017.06.016.
[14] Q. Liu, Q. Xu, Q. Yu, R. Gao, T. Tong, Experimental investigation on mechanical and piezoresistive properties of cementitious materials containing graphene and graphene oxide nanoplatelets, Constr. Build. Mater. 127 (2016) 565–576, https://doi.org/10.1016/j.conbuildmat.2016.10.024.
[15] W. Baomin, D. Shuang, Effect and mechanism of graphene nanoplatelets on hydration reaction, mechanical properties and microstructure of cement composites, Constr. Build. Mater. 228 (2019), https://doi.org/10.1016/j.conbuildmat.2019.116720.
[16] J. Tao, X. Wang, Z. Wang, Q. Zeng, Graphene nanoplatelets as an effective additive to tune the microstructures and piezoresistive properties of cement-based composites, Constr. Build. Mater. 209 (2019) 665–678, https://doi.org/10.1016/j.conbuildmat.2019.03.173.
[17] Z. Jiang, M.M. Sherif, G. Xing, O.E. Ozbulut, Tensile characterization of graphene nanoplatelets (GNP) mortar using acoustic emissions, Mater. Today Commun. 25 (2020), https://doi.org/10.1016/j.mtcomm.2020.101433.
[18] G. Chen, M. Yang, L. Xu, Y. Zhang, Y. Wang, Graphene nanoplatelets impact on concrete in improving freeze-thaw resistance, Appl. Sci. (Switz.) 9 (2019), https://doi.org/10.3390/app9173582.
[19] B. Wang, D. Shuang, Effect of graphene nanoplatelets on the properties, pore structure and microstructure of cement composites, Mater. Express 8 (2018) 407–416, https://doi.org/10.1166/mex.2018.1447.
[20] H. Alkhateb, A. Al-Ostaz, A.H.-D. Cheng, X. Li, Materials genome for graphene-cement nanocomposites, J. Nanomech. Micromech. 3 (2013) 67–77, https://doi.org/10.1061/(asce)nm.2153-5477.0000055.
[21] Q. Zheng, B. Han, X. Cui, X. Yu, J. Ou, Graphene-engineered cementitious composites: small makes a big impact, Nanomater. Nanotechnol. 7 (2017), https://doi.org/10.1177/1847980417742304.
[22] N. Jaitanong, S. Narksitipan, A. Ngamjarurojana, A. Chaipanich, Influence of graphene nanoplatelets on morphological and electrical properties of silica fume blended cement – Piezoelectric ceramic composite, Ceram. Int 44 (2018) S137–S140, https://doi.org/10.1016/j.ceramint.2018.08.131.
[23] M.N. Noorsuhada, An overview on fatigue damage assessment of reinforced concrete structures with the aid of acoustic emission technique, Constr. Build. Mater. 112 (2016) 424–439, https://doi.org/10.1016/j.conbuildmat.2016.02.206.
[24] M. Ohtsu, M. Shigeishi, H. Iwaset, W. Koyanagit K U M A M O T, Determination of crack location, type 4. and orientation in concrete structures acoustic ernlsslon, 1991.
[25] E. Proverbio, Evaluation of deterioration in reinforced concrete structures by AE technique, Mater. Corros. 62 (2011) 161–169, https://doi.org/10.1002/maco.201005735.
[26] H.A. Elfergani, R. Pullin, K.M. Holford, Damage assessment of corrosion in prestressed concrete by acoustic emission, Constr. Build. Mater. 40 (2013) 925–933, https://doi.org/10.1016/j.conbuildmat.2012.11.071.
[27] S. Shahidan, R. Pulin, N. Muhamad Bunnori, K.M. Holford, Damage classification in reinforced concrete beam by acoustic emission signal analysis, Constr. Build. Mater. 45 (2013) 78–86, https://doi.org/10.1016/j.conbuildmat.2013.03.095.
[28] A. Carpinteri, G. Lacidogna, A. Manuello, The b-Value analysis for the stability investigation of the ancient athena temple in syracuse, Strain 47 (2011), https://doi.org/10.1111/j.1475-1305.2008.00602.x.
[29] I.S. Colombo, I.G. Main, M.C. Forde, Assessing Damage of Reinforced Concrete Beam Using '"b-value'" Analysis of Acoustic Emission Signals, (n.d.). https://doi.org/10.1061/ASCE0899–1561200315:3280.
[30] T. Shiotani, M. Ohtsu, K. Ikeda, Detection and evaluation of AE waves due to rock deformation, n.d.
[31] R.V. Sagar, B.K.R. Prasad, S.S. Kumar, An experimental study on cracking evolution in concrete and cement mortar by the b-value analysis of acoustic emission technique, Cem. Concr. Res 42 (2012) 1094–1104, https://doi.org/10.1016/j.cemconres.2012.05.003.
[32] Q. Han, G. Yang, J. Xu, Z. Fu, G. Lacidogna, A. Carpinteri, Acoustic emission data analyses based on crumb rubber concrete beam bending tests, Eng. Fract. Mech. 210 (2019) 189–202, https://doi.org/10.1016/j.engfracmech.2018.05.016.
[33] A. Loukidis, D. Triantis, I. Stavrakas, E.D. Pasiou, S.K. Kourkoulis, Comparative Ib-value and F-function analysis of Acoustic Emissions from elementary and structural tests with marble specimens, Material Design and Processing, Communications 3 (2021), https://doi.org/10.1002/mdp2.176.
[34] S. Yuyama, Z.-W. Li, Y. Ito, M. Arazoe, Quantitative analysis of fracture process in RC column foundation by moment tensor analysis of acoustic emission, n.d.
[35] M.A.A. Aldahdooh, N.Muhamad Bunnori, Crack classification in reinforced concrete beams with varying thicknesses by mean of acoustic emission signal features, Constr. Build. Mater. 45 (2013) 282–288, https://doi.org/10.1016/j.conbuildmat.2013.03.090.
[36] J. Xu, S. Ashraf, S. khan, X. Chen, A. Akbar, F. Farooq, Micro-cracking pattern recognition of hybrid CNTs/GNPs cement pastes under three-point bending loading using acoustic emission technique, J. Build. Eng. 42 (2021), https://doi.org/10.1016/j.jobe.2021.102816.
[37] A. Nair, Acoustic emission monitoring and quantitative evaluation of Acoustic emission monitoring and quantitative evaluation of damage in reinforced concrete members and bridges damage in reinforced concrete members and bridges, n.d. ⟨https://digitalcommons.lsu.edu/gradschool_theses⟩.
[38] S. Degala, P. Rizzo, K. Ramanathan, K.A. Harries, Acoustic emission monitoring of CFRP reinforced concrete slabs, Constr. Build. Mater. 23 (2009) 2016–2026, https://doi.org/10.1016/j.conbuildmat.2008.08.026.
[39] A.A. Abouhussien, A.A.A. Hassan, Classification of damage in self-consolidating rubberized concrete using acoustic emission intensity analysis, Ultrasonics 100 (2020), https://doi.org/10.1016/j.ultras.2019.105999.
[40] Q. Han, L. Wang, J. Xu, A. Carpinteri, G. Lacidogna, A robust method to estimate the b-value of the magnitude-frequency distribution of earthquakes, Chaos Solitons Fractals 81 (2015) 103–110, https://doi.org/10.1016/j.chaos.2015.09.004.
[41] B. Gutenberg, C.F. Richter, Frequency of earthquakes in California, Bull. Seismol. Soc. Am. 34 (1944) 185–188.
[42] A. Carpinteri, G. Lacidogna, S. Puzzi, From criticality to final collapse: evolution of the "b-value" from 1.5 to 1.0, Chaos Solitons Fractals 41 (2009) 843–853, https://doi.org/10.1016/j.chaos.2008.04.010.
[43] D.G. Aggelis, D. v Soulioti, N. Sapouridis, N.M. Barkoula, A.S. Paipetis, T.E. Matikas, Acoustic emission characterization of steel fibre reinforced concrete during bending. Nondestructive Characterization for Composite Materials, Aerospace Engineering, Civil Infrastructure, and Homeland Security 2010, SPIE,, 2010, 764912, https://doi.org/10.1117/12.847396.
[44] D.G. Aggelis, Classification of cracking mode in concrete by acoustic emission parameters, Mech. Res Commun. 38 (2011) 153–157, https://doi.org/10.1016/j.mechrescom.2011.03.007.
[45] M. di Benedetti, A. Nanni, Acoustic emission intensity analysis for in-situ evaluation of reinforced concrete slab 1 2 by 3 4, n.d.
[46] D.S. Li, C. Hai, O. Jinping, Fracture behavior and damage evaluation of polyvinyl alcohol fiber concrete using acoustic emission technique, Mater. Des. 40 (2012) 205–211, https://doi.org/10.1016/j.matdes.2012.03.051.
[47] S. Chuah, W. Li, S.J. Chen, J.G. Sanjayan, W.H. Duan, Investigation on dispersion of graphene oxide in cement composite using different surfactant treatments, Constr. Build. Mater. 161 (2018) 519–527, https://doi.org/10.1016/j.conbuildmat.2017.11.154.
[48] B. Wang, R. Jiang, W. Song, H. Liu, Controlling dispersion of graphene nanoplatelets in aqueous solution by ultrasonic technique, Russ. J. Phys. Chem. A 91 (2017) 1517–1526, https://doi.org/10.1134/S0036024417080040.
[49] M.T.H. Aunkor, I.M. Mahbubul, R. Saidur, H.S.C. Metselaar, Deoxygenation of graphene oxide using household baking soda as a reducing agent: a green approach, RSC Adv. 5 (2015) 70461–70472, https://doi.org/10.1039/c5ra10520j.
[50] I.K. Tragazikis, K.G. Dassios, D.A. Exarchos, P.T. Dalla, T.E. Matikas, Acoustic emission investigation of the mechanical performance of carbon nanotube-modified cement-based mortars, Constr. Build. Mater. 122 (2016) 518–524, https://doi.org/10.1016/j.conbuildmat.2016.06.095.
[51] R.Vidya Sagar, Acoustic emission characteristics of reinforced concrete beams with varying percentage of tension steel reinforcement under flexural loading, Case Stud. Constr. Mater. 6 (2017) 162–176, https://doi.org/10.1016/j.cscm.2017.01.002.